

Non-Hermitian tearing by dissipation

Qian Du¹, Xin-Ran Ma², Su-Peng Kou^{2*}

¹School of Physics and Electronic Engineering, Linyi University, Linyi, 276000, China.

²Center for Advanced Quantum Studies, Department of Physics, Beijing Normal University, Beijing, 100875, China.

*Corresponding author(s). E-mail(s): spkou@bnu.edu.cn;

Abstract

In the paper, we study the non-Hermitian system under dissipation and give the effective 2×2 Hamiltonian in the \mathbf{k} -space by reducing the $N \times N$ Hamiltonian in the real space for them. It is discovered that the energy band shows an imaginary line gap. To describe these phenomena, we propose the theory of “non-Hermitian tearing”, in which the tearability we define reveals a continuous phase transition at the exceptional point. The non-Hermitian tearing manifests in two forms — separation of bulk state and decoupling of boundary state. In addition, we also explore the one-dimensional Su-Schrieffer-Heeger model and the Qi-Wu-Zhang model under dissipation using the theory of non-Hermitian tearing. Our results provide a theoretical approach for exploring the controlling of non-Hermitian physics on topological quantum states.

Keywords: non-Hermitian systems, dissipation, topological insulators, open quantum systems

1 Introduction

Non-Hermitian systems have been a hot topic owing to their unique properties and potential applications in various fields, such as optics [1–8], condensed matter physics [9–16], and quantum mechanics [17–20]. In the fundamental principles of quantum mechanics, the physical quantity describing the state of a microscopic system is a Hermitian operator in Hilbert space, whose expected value is a real number. However, in practice, we find that the probability of a system does not always conserve, and the eigenvalues of energy can also be complex [21–23]. Thus, non-Hermitian operators

become crucial. The origins of the non-Hermitian Hamiltonian can be traced back to the lifetime of a quasiparticle [24–26], columnar defects in the superconductor [27], and so on. Gradually, people’s understanding of quantum mechanics extended from Hermitian systems to non-Hermitian systems.

In recent years, non-Hermitian physics has witnessed remarkable advancement. Bender pointed out in 1998 that the energy spectrum of a Hamiltonian satisfying parity-time (\mathcal{PT}) symmetry can be classified into three cases: all real numbers, complex conjugate pairs, and a situation with spectral degeneracy and eigenstates merging, which is known as \mathcal{PT} -symmetry spontaneously broken [28]. This discovery has inspired an array of theoretical and experimental breakthroughs in non-Hermitian physics, including the non-Hermitian skin effect [29–34] and the breakdown of bulk-boundary correspondence [33, 35–40]. There has been a great deal of research focused on non-Hermitian systems with global non-Hermitian terms, such as gain and loss [41–44] and nonreciprocal hopping [44–47], or the local non-Hermitian terms [48, 49]. In particular, Ref. [41] demonstrated the arbitrary, robust light steering in reconfigurable non-Hermitian gain–loss junctions by projecting the designed spatial pumping patterns onto the photonic topological lattice. Ref. [42] studied photonic topological insulators with different types of gain-loss domain walls and proposed an effective Hamiltonian describing localized states and the corresponding energies occurring at the domain walls. However, there are still many problems worth studying. For example, how exactly do the bulk states change with non-Hermitian terms? How do the boundary states appear and change? Previous studies have mainly focused on the occurrence of boundary states with gain and loss, while the physical properties of other states were not considered. In this paper, we not only study the changes of boundary states, but also the properties of bulk states. We systematically investigate the properties of bulk states and boundary states under dissipation, especially the characteristics of boundary states after bulk states are separated by gain and loss.

In the paper, we study an arbitrary one-dimensional tight binding model under dissipation where the left and right sites are subject to different imaginary potentials and give a series of effective 2×2 Hamiltonians $h_{\text{eff}}(k)$ in the k -space by reducing the $N \times N$ Hamiltonian in the real space to understand it. It is shown that the original single band is divided into two energy bands and then appears an imaginary line gap. To describe these novel phenomena, we propose the concept of “non-Hermitian tearing”, in which the system is either in the partial tearing or in the complete tearing. During these processes, the energy eigenvalues display a \mathcal{PT} transition. Furthermore, we define the tearability to characterize the effect of different imaginary potentials on an eigenstate. According to the relationship between the direction of wave vectors and the interface’s direction, we introduce two types of non-Hermitian tearing — separation and decoupling. Using the theory of non-Hermitian tearing, we explore the physical properties of a simple one-dimensional tight binding model, the one-dimensional Su-Schrieffer-Heeger (SSH) model and the Qi-Wu-Zhang (QWZ) model. The results indicated that the tearability exhibits a continuous phase transition at the exceptional point. Bulk states show separation and boundary states show decoupling. We give the effective Hamiltonian of bulk states and boundary states for them, which

fits well with numerical solutions. Our study contributes a theoretical approach to studying physical properties in more complex non-Hermitian systems.

The outline of this paper is as follows. In Sec. 2, based on an arbitrary one-dimensional tight binding model with the imaginary potential, we give a series of effective 2×2 Hamiltonians in the k -space by reducing the $N \times N$ Hamiltonian in the real space to understand it. From this, we propose the theory of non-Hermitian tearing. In Sec. 3, we take a simple one-dimensional tight binding model as an example to explore the physical properties of non-topological systems with the imaginary potential by the theory of non-Hermitian tearing. In Sec. 4, we study the non-Hermitian tearing in the one-dimensional SSH model and discover that two pairs of boundary states appear after bulk states are separated. Moreover, these boundary states also show non-Hermitian tearing with a \mathcal{PT} transition. In Sec. 5, we discuss the same issue in the QWZ model. In Sec. 6, we draw the conclusion.

2 Non-Hermitian tearing

We consider an arbitrary one-dimensional tight binding model H_0 with a negative imaginary potential $-iv$ on the left $N/2$ sites and a positive imaginary potential iv on the right $N/2$ sites under the periodic boundary condition. The adjacent part between different imaginary potentials is named the interface. To better understand the physical phenomena of the total system, we give the effective Hamiltonian H_{eff} in the k -space by reducing the $N \times N$ Hamiltonian in the real space, which is composed of a series of effective 2×2 Hamiltonians $h_{\text{eff}}(k)$.

Theorem 1 (The effective Hamiltonian). *The effective 2×2 Hamiltonian $h_{\text{eff}}(k)$ can be written as*

$$h_{\text{eff}}(k) = \begin{pmatrix} h_0(k) - iv & \frac{\alpha(k)}{\sqrt{N_1}} \\ \frac{\alpha(k)}{\sqrt{N_1}} & h_0(k) + iv \end{pmatrix} \quad (1)$$

for $k = 2\pi j/N_1$, $j = 1, 2, \dots, N_1$ and $N_1 = N/2$, where $h_0(k)$ is the Hamiltonian of H_0 in the k -space and v is the imaginary potential strength. $\alpha(k)$ represents the coupling term at the interface, which is a k -dependent real number.

The eigenvalue of the effective Hamiltonian is

$$E_{\text{eff}}(k) = E_0(k) \pm \sqrt{\frac{\alpha^2(k)}{N_1} - v^2}, \quad (2)$$

where $E_0(k)$ is the eigenvalue of $h_0(k)$. Obviously, there is the \mathcal{PT} transition. For a given k , as $\alpha^2(k) > N_1 v^2$, $E_{\text{eff}}(k)$ is all real and the eigenvalues are in the phase with \mathcal{PT} -symmetry; as $\alpha^2(k) = N_1 v^2$, $E_{\text{eff}}(k) = E_0(k)$, the eigenvalues occurs the \mathcal{PT} -symmetric spontaneous breaking; as $\alpha^2(k) < N_1 v^2$, $E_{\text{eff}}(k)$ is all complex and the eigenvalues in the phase with \mathcal{PT} -symmetry breaking. With increasing v , the eigenvalues transition from all real to all complex. In the case of $\alpha^2(k) \ll N_1 v^2$ for all k , all eigenvalues are complex and the original single band $E_0(k)$ is divided into one energy band with a negative imaginary part $-i\sqrt{v^2 - \frac{\alpha^2(k)}{N_1}}$ and one energy band with

a positive imaginary part $i\sqrt{v^2 - \frac{\alpha^2(k)}{N_1}}$. An imaginary line gap $\Delta = 2i\sqrt{v^2 - \frac{\alpha^2(k)}{N_1}}$ appears between these two energy bands. In order to describe the phenomenon, we give the following definitions:

Definition 1 (Non-Hermitian tearing). *If the original single band of the system is gradually divided into two energy bands due to the imaginary potential, a down energy band E_{down} and an up energy band E_{up} , then an imaginary line energy gap emerges between these two energy bands,*

$$\Delta = \min(\text{Im } E_{\text{up}}) - \max(\text{Im } E_{\text{down}}). \quad (3)$$

The phenomenon is called “non-Hermitian tearing”.

In terms of the presence or absence of the imaginary line energy gap, we give *partial tearing* and *complete tearing*.

Definition 2 (Partial tearing and complete tearing). *If all energy eigenvalues are complex and the imaginary line energy gap is present, $\Delta > 0$, then we think that the system is in the “complete tearing”. If some energy eigenvalues are still real and the imaginary line energy gap is absent, $\Delta = 0$, then we think that the system is in the “partial tearing”.*

In particular, when the system crosses over the critical point between the partial tearing and complete tearing, the energy spectrum shows a \mathcal{PT} transition.

For one of these eigenvalues, to characterize the effect of different imaginary potentials on its corresponding eigenstate, we introduce the *tearability*:

Definition 3 (Tearability). *The ratio of the probability of an eigenstate $\Psi_j = (\psi_1, \dots, \psi_n, \dots, \psi_N)^\dagger$ in the right $N/2$ sites and left $N/2$ sites is defined as the tearability of this eigenstate*

$$t_j = \frac{\rho_{j,\text{R}}}{\rho_{j,\text{L}}}, \quad (4)$$

where

$$\rho_{j,\text{L}} = \sum_{n=1}^{N/2} |\psi_n|^2, \quad \rho_{j,\text{R}} = \sum_{n=N/2+1}^N |\psi_n|^2. \quad (5)$$

Ψ_j is the right basis of Hamiltonian of the total system. Thus, $\rho_{j,\text{L}} + \rho_{j,\text{R}} = 1$.

$t_j = 1$ means that the probability in the right $N/2$ sites is the same as the probability in the left $N/2$ sites and the eigenstate is not torn. On the contrary, $t_j \neq 1$ means that the probability in the right $N/2$ sites are different from the probability in the left $N/2$ sites and the eigenstate is torn. $t_j \rightarrow 0$ or $t_j \rightarrow \infty$ means that the corresponding wave function is bound in the left $N/2$ sites or right $N/2$ sites and the eigenstate is strongly torn.

In the non-Hermitian tearing, we think that the interface is directional. Its direction in the one-dimensional tight binding model is identified as the y -direction. We assume that the wave function corresponding to the eigenstate is a plane wave and k is the wave vector. According to the relationship between the interface’s direction and the direction of k , we define *separation* and *decoupling*.

Definition 4 (Separation and decoupling). *If the direction of the wave vector of the eigenstate is perpendicular to the interface’s direction, then we call such a non-Hermitian tearing “separation” and the wave vector is denoted by k_\perp . Conversely, if*

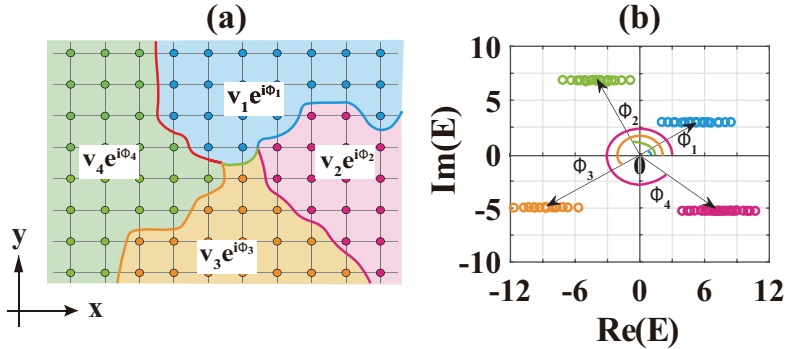


Fig. 1 The two-dimensional square lattice model with uniform hopping under the periodic boundary conditions along the x-direction and y-direction. The four different complex potentials are $v_1e^{i\phi_1}$, $v_2e^{i\phi_2}$, $v_3e^{i\phi_3}$, and $v_4e^{i\phi_4}$, respectively. (a) The model diagram. (b) The energy spectrum. Here, $v_1 = 6$, $v_2 = 8$, $v_3 = 10$, $v_4 = 9$, and $\phi_1 = \frac{\pi}{6}$, $\phi_2 = \frac{2\pi}{3}$, $\phi_3 = \frac{7\pi}{6}$, $\phi_4 = \frac{9\pi}{5}$.

the direction of the wave vector of the eigenstate is parallel to the interface's direction, then we call such a non-Hermitian tearing “decoupling” and the wave vector is denoted by $k_{//}$.

Given a more general case, a complex potential is applied to the two-dimensional non-topological model

$$V = v_1e^{i\phi_1} \sum_{n=1}^{N_1} c_n^\dagger c_n + v_2e^{i\phi_2} \sum_{n=N_1+1}^{N_1+N_2} c_n^\dagger c_n + \cdots + v_me^{i\phi_m} \sum_{n=N_1+\cdots+N_{m-1}+1}^{N_1+\cdots+N_{m-1}+N_m} c_n^\dagger c_n, \quad (6)$$

where the real number $v_{1,2,\dots,m}$ represents the magnitudes of the m different complex potentials and $\phi_{1,2,\dots,m}$ is the corresponding phase angle with $\phi_{1,2,\dots,m} \in [0, 2\pi]$. Here, $N = N_1 + N_2 + \cdots + N_m$. In the system, the complex potential $v_1e^{i\phi_1}$ is applied to the N_1 sites, the complex potential $v_2e^{i\phi_2}$ is applied to the N_2 sites, and so on. Using a two-dimensional square lattice model as an example, we consider the complex potential as shown in Fig. 1(a), and show the complex energy spectrum in Fig. 1(b). The energy spectrum of the system is torn to different positions along different directions, depending on the form of the complex potential. Explicitly, the direction is the phase angle of the complex potential, and the position is relevant to the amplitude of the complex potential.

In the following sections, we will explore the physical properties of the simple one-dimensional tight binding model, the one-dimensional SSH model, and the QWZ model with the imaginary potential based on the theory of non-Hermitian tearing.

3 The simple one-dimensional tight binding model with the imaginary potential

In this part, we mainly discuss the simple one-dimensional tight binding model with the imaginary potential by the theory of non-Hermitian tearing to investigate the effect of the imaginary potential on non-topological systems.

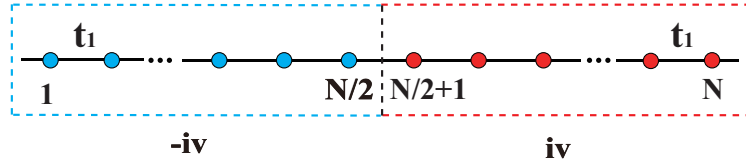


Fig. 2 Illustration of the simple one-dimensional tight binding model with the negative potential $-iv$ on the left $N_1 = N/2$ sites and the positive potential iv on the remaining sites. t_1 represents hopping amplitude.

The Hamiltonian of the simple one-dimensional tight binding model in real space is

$$H_0 = t_1 \sum_{n=1}^N c_n^\dagger c_{n+1} + h.c., \quad (7)$$

where t_1 represents the hopping amplitude of an electron jumping from site n to site $n + 1$. c_n^\dagger and c_n are the creation and annihilation operators of electron at site n , respectively. The Hamiltonian in the k -space is

$$h_0(k) = 2t_1 \cos k, \quad (8)$$

and its eigenvalue is

$$E_0 = 2t_1 \cos k. \quad (9)$$

We consider the imaginary potential

$$V = -iv \sum_{n=1}^{N/2} c_n^\dagger c_n + iv \sum_{n=N/2+1}^N c_n^\dagger c_n \quad (10)$$

for the model, as shown in Fig. 2. In the paper, we use t_1 as the unit.

Figure 3 plots the system's complex energy spectra and eigenstates for different imaginary potential strength v under the periodic boundary condition. One can see that as v goes up, the eigenvalues gradually move along the positive or negative direction of the imaginary axis. Upon reaching a particular imaginary potential, one energy band of the system is divided into two energy bands: an up band E_{up} with a positive imaginary part and a down band E_{down} with a negative imaginary part, as shown in Fig. 3(c). As a consequence, an imaginary line gap appears between the two energy bands. This indicates that the simple one-dimensional tight binding model with the imaginary potential shows non-Hermitian tearing. In particular, there is a \mathcal{PT} transition in which the system transitions from partial tearing to complete tearing in Fig. 3(b). Blue circles (red circles) represent the energy eigenvalues moving along the negative (positive) direction of the imaginary axis, and black circles represent unmoved energy eigenvalues. The wave functions of moved energy eigenvalues (depicted by the blue curve or the red curve) are bound to the left $N/2$ sites or the right $N/2$ sites, while the wave functions of unmoved energy eigenvalues (depicted by the black curve) still spread across all sites. In Fig. 3(a), some energy eigenvalues are still real and the

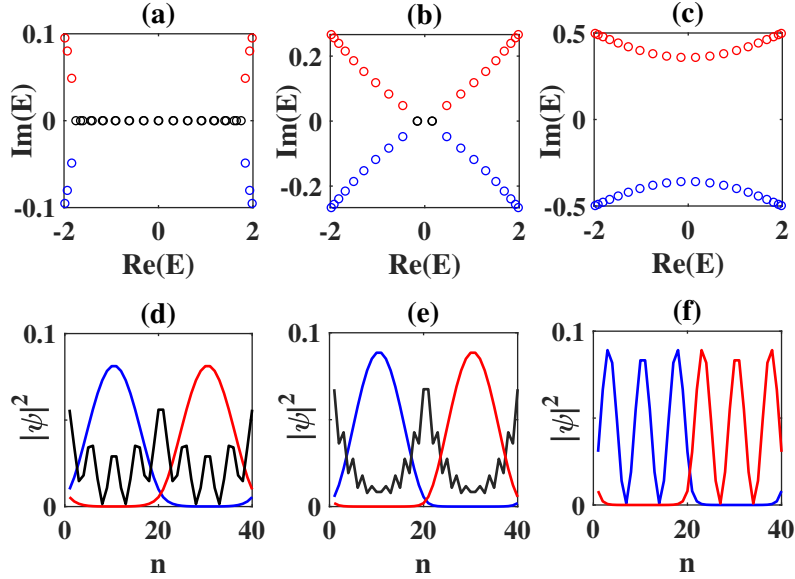


Fig. 3 (a), (b) and (c) are complex energy spectra for different imaginary potential strengths $v = 0.1, 0.2695$ and 0.5 , respectively. (d), (e) and (f) are the corresponding bulk states versus site n , respectively. The red, black or blue curve is a representative wave function of energy eigenvalues represented by red, black or blue circles. Here, $t_1 = 1$ and $N = 40$.

imaginary line energy gap is absent, so the system is in the partial tearing. In Fig. 3(c), all energy eigenvalues are complex and the imaginary line energy gap is present, so the system is in the complete tearing. Note that these energy eigenstates are bulk states and the directions of their wave vectors are perpendicular to the interface's direction, so bulk states show separation.

Considering that the energy eigenvalues move along the imaginary axis, we arrange it in ascending order by imaginary part, $E_1, \dots, E_j, \dots, E_N$, and show the corresponding probability in Fig. 4. The probabilities of energy eigenvalues moving along the negative (positive) direction of the imaginary axis are $\rho_L > \rho_R$ ($\rho_L < \rho_R$), whereas the probabilities of unmoved energy eigenvalues are $\rho_L = \rho_R = 0.5$. Together with Figs. 3(b) and 3(c), we can find that in the partial tearing, there are some eigenstates with $t = 1$ that correspond to unmoved energy eigenvalues and are not torn. In the complete tearing, all eigenstates have $t \neq 1$ and are torn at the left $N/2$ sites or the right $N/2$ sites.

Further, we calculate the tearability t of the $j = 11$ and the $j = 31$ bulk states in Figs. 5(a) and (c), respectively. The tearability $t = 1$ indicates that the bulk state is in the phase with \mathcal{PT} symmetry and the tearability $t \rightarrow 0$ or $t \rightarrow \infty$ indicates that the bulk state is in the phase with \mathcal{PT} -symmetry breaking. They are continuous at the exceptional point where their energy eigenvalues transition from real numbers to complex numbers. Later on, we calculate their derivatives $\frac{\partial t}{\partial v}$ in Figs. 5(b) and (d). $\frac{\partial t}{\partial v}$ is discontinued at the exceptional point, which means a second-order phase transition at the exceptional point.

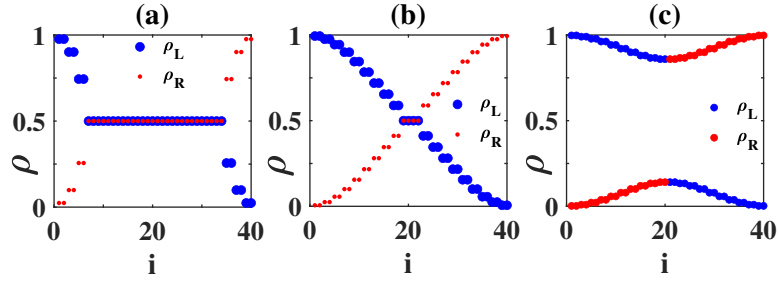


Fig. 4 The probability of the simple one-dimensional tight binding model with the imaginary potential, where i is the sort number. (a), (b) and (c) are the probabilities for different imaginary potential strengths $v = 0.1, 0.2695$ and 0.5 , respectively. Here, $t_1 = 1$ and $N = 40$.

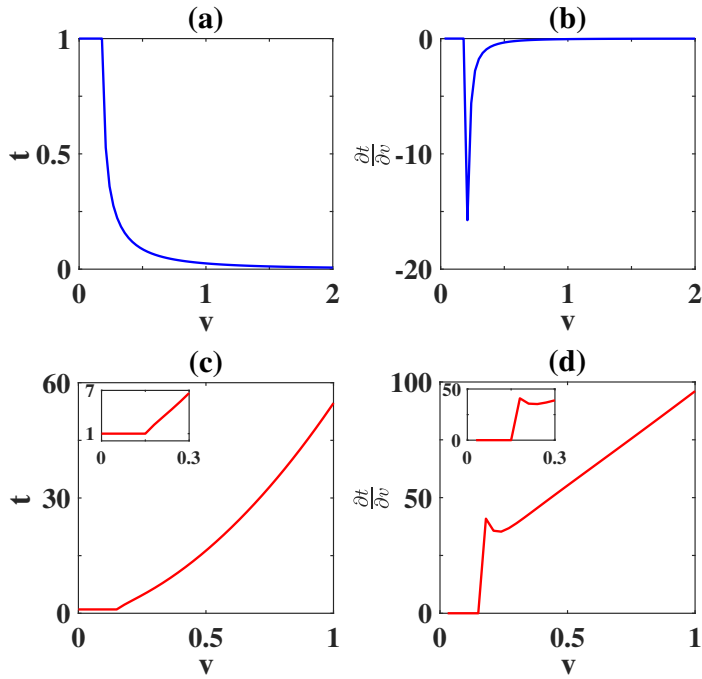


Fig. 5 (a) and (b) are the tearability t and the derivative $\frac{\partial t}{\partial v}$ of the $j = 11$ bulk state, respectively. (c) and (d) are the tearability t and derivative $\frac{\partial t}{\partial v}$ of the $j = 31$ bulk state, respectively. Here, $t_1 = 1$ and $N = 40$.

According to Theorem 1 in Eq. (1), we give the effective Hamiltonian $h_{\text{eff}}(k)$ of bulk states

$$h_{\text{eff}}(k) = \begin{pmatrix} h_0(k) - iv & \frac{\alpha(k)}{\sqrt{N_1}} \\ \frac{\alpha(k)}{\sqrt{N_1}} & h_0(k) + iv \end{pmatrix}, \quad (11)$$

where $\alpha(k) = h_0(k + \frac{3\pi}{2}) \cdot \lambda = 2t_1 \sin k/\lambda$ and λ is a fitting parameter related to v . Here, $k = 2\pi j/N_1$, $j = 1, 2, \dots, N_1$ and $N_1 = N/2$. We plot the complex energy spectrum from analytical solutions of the effective Hamiltonian H_{eff} in the k -space and

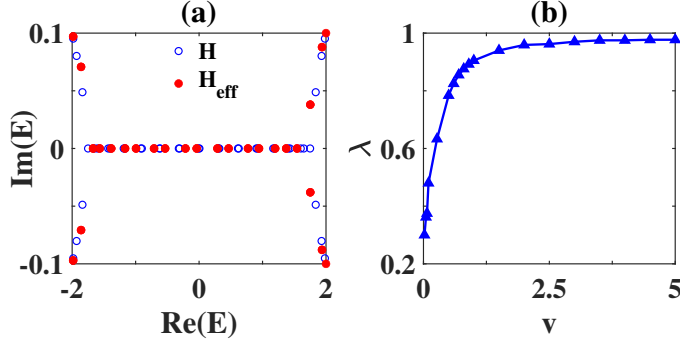


Fig. 6 (a) The complex energy spectrum from numerical solutions of the Hamiltonian H in the real space and analytical solutions of the effective Hamiltonian H_{eff} in the k -space, where $v = 0.1$ and $\lambda = 0.493$. (b) The fitting parameter λ versus the imaginary potential strength v . Here, $t_1 = 1$ and $N = 40$.

numerical solutions of the Hamiltonian $H = H_0 + V$ in the real space in Fig. 6(a). It can be seen that the effective Hamiltonian fits well with numerical solutions, demonstrating that the Theorem 1 we give can well describe the properties of one-dimensional tight binding models with the imaginary potential. See the detailed calculations regarding the probability and tearability of eigenstates of $h_{\text{eff}}(k)$ in Appendix A. The imaginary line gap is

$$\Delta = 2\sqrt{\frac{4t_1^2\lambda^2\sin^2 k}{N_1} - v^2}. \quad (12)$$

As $\frac{4t_1^2\lambda^2\sin^2 k}{N_1} - v^2 = 0$, namely,

$$k = k_0 = \pm \arcsin \frac{v\sqrt{N_1}}{2t_1\lambda}, \quad (13)$$

we have $E_{\text{eff}}(k_0) = E_0(k_0)$ and the bulk state is at the \mathcal{PT} transition. Besides, we show the fitting parameter λ as a function of v in Fig. 6(b). It can be seen that when v is increased to a large value, λ reaches a saturation value 1. In particular, if this model with the real potential, then the eigenvalues are all real and it does not show the \mathcal{PT} transition from Eq. (11). When the system is torn, the tearability does not have a second-order continuous phase transition and is only at a crossover.

4 The one-dimensional Su-Schrieffer-Heeger model with the imaginary potential

In this section, we take the one-dimensional SSH model as an example and explore the physical properties of one-dimensional topological systems with imaginary potential.

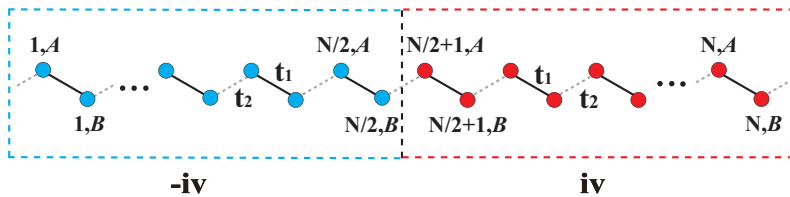


Fig. 7 The one-dimensional Su-Schrieffer-Heeger model with the negative potential $-iv$ on the left $N/2$ pairs of lattice sites and the positive potential iv on the right $N/2$ pairs of lattice sites. t_1 and t_2 describe the intra-cell and inter-cell hopping strengths, respectively.

The Hamiltonian of the one-dimensional SSH model in the real space is

$$H_{\text{SSH}} = t_1 \sum_{n=1}^N |n, B\rangle \langle n, A| + t_2 \sum_{n=1}^{N-1} |n+1, A\rangle \langle n, B| + h.c., \quad (14)$$

where A and B denote the two sublattices of each pair of lattice sites. t_1 and t_2 describe the intra-cell and inter-cell hopping strengths, respectively. Here, we use t_1 as the unit and set $t_2 = 2t_1 = 2$. The Hamiltonian in k -space is

$$h_{\text{SSH}}(k) = (t_1 + t_2 \cos k) \sigma_x + (t_2 \sin k) \sigma_y, \quad (15)$$

where σ_i 's are the Pauli matrices acting on the sublattice subspace. Its eigenvalue in the k -space is

$$E_{\pm}(k) = \pm \sqrt{(t_1 + t_2 \cos k)^2 + (t_2 \sin k)^2}. \quad (16)$$

Here, we consider the imaginary potential

$$V = -iv \sum_{n=1}^{N/2} (|n, A\rangle \langle n, A| + |n, B\rangle \langle n, B|) + iv \sum_{n=N/2+1}^N (|n, A\rangle \langle n, A| + |n, B\rangle \langle n, B|) \quad (17)$$

for the model as shown in Fig. 7.

Figures 8 and 9 plot the complex energy spectra and eigenstates for different imaginary potential strengths v under the periodic boundary condition. With increasing v , each energy band of the system is gradually divided into two energy bands: an up band E_{up} with a positive imaginary part and a down band E_{down} with a negative imaginary part, as shown in Fig. 9. An imaginary line gap emerges between the two energy bands, meaning that the one-dimensional SSH model with the imaginary potential shows non-Hermitian tearing accompanied by the \mathcal{PT} transition. In addition, bulk states show separation.

Surprisingly, after the bulk states are separated, the system appears two pairs of boundary states as depicted in Fig. 9. As the imaginary potential strength v grows further, these two pairs of boundary states also show non-Hermitian tearing along with a \mathcal{PT} transition. Eventually, the wave function of the boundary state corresponding

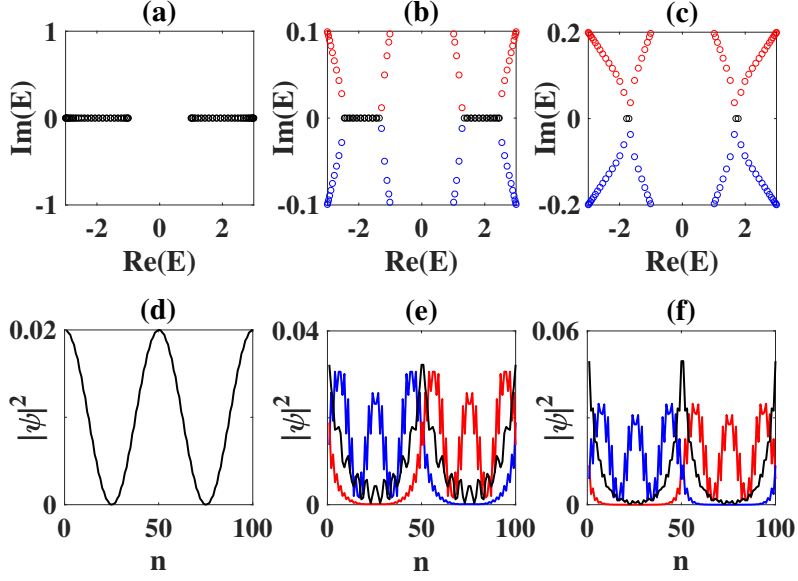


Fig. 8 (a), (b) and (c) are the complex energy spectra for different imaginary potential strengths $v = 0, 0.1$ and 0.2 , respectively. (d) to (f) are the corresponding bulk states versus site n . The red, black or blue curve is a representative wave function of energy eigenvalues represented by red, black or blue circles. Here, $t_1 = 1, t_2 = 2$, and $N = 50$.

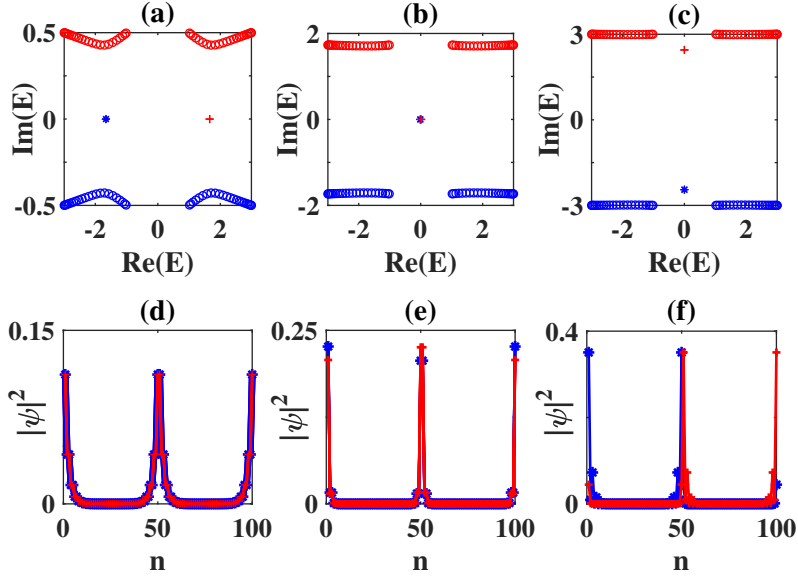


Fig. 9 (a), (b) and (c) are the complex energy spectra for different imaginary potential strengths $v = 0.5, 1.732$ and 3 , respectively. (d), (e) and (f) are one of the left (depicted by a blue curve with asterisks) and right (depicted by a red curve with plus signs) boundary states, respectively. Here, $t_1 = 1, t_2 = 2$, and $N = 50$.

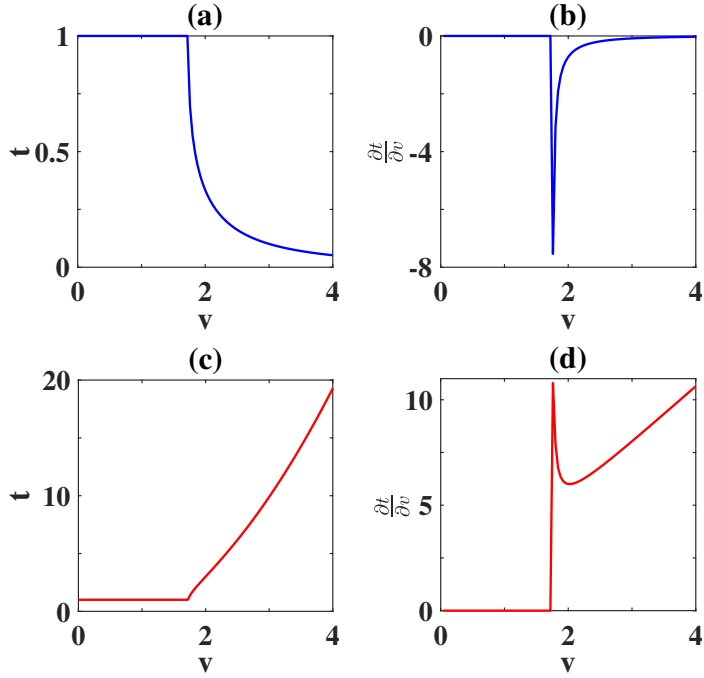


Fig. 10 (a) and (b) are the tearability t and the derivative $\frac{\partial t}{\partial v}$ versus the imaginary potential strength v of the first boundary state, respectively. (c) and (d) are the tearability t and the derivative $\frac{\partial t}{\partial v}$ versus as the imaginary potential strength v of the fourth boundary state, respectively. Here, $t_1 = 1$ and $N = 40$.

to the down energy band (represented by blue asterisks), which is depicted by the blue curve with asterisks, is localized on the two boundaries of the left $N/2$ pairs of lattice sites in Fig. 9(f). The wave function of the boundary state corresponding to the up energy band (represented by red plus signs), which is depicted by the red curve with red plus signs, is localized on the two boundaries of the right $N/2$ pairs of lattice sites. The directions of wave vectors of these boundary states are parallel to the interface's direction, so these boundary states show decoupling.

To further investigate the non-Hermitian tearing of boundary states, we select one of these two pairs of boundary states and calculate the tearability t as a function of the imaginary potential strength v in Figs. 10(a) and (c), respectively. As $t = 1$, the boundary state is not torn and its energy eigenvalue is in the phase with \mathcal{PT} -symmetry, whereas as $t \rightarrow 0$ or $t \rightarrow \infty$, the boundary state is torn and its energy eigenvalue in the phase with \mathcal{PT} -symmetry breaking. The tearability is continuous at the exceptional point where their energy eigenvalues transition from real numbers to imaginary numbers. Later on, we display their derivatives $\frac{\partial t}{\partial v}$ versus v in Figs. 10(b) and (d). It is evident that $\frac{\partial t}{\partial v}$ is discontinued at the exceptional point, which implies that tearability has a second-order phase transition at the exceptional point.

According to Theorem 1 in Eq. (1), we give the effective Hamiltonian of bulk states and boundary states, respectively. Firstly, the effective Hamiltonian of bulk states can

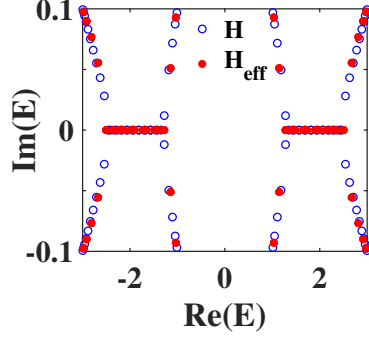


Fig. 11 The complex energy spectrum from numerical solutions of the Hamiltonian H in the real space and the analytical solutions of the effective Hamiltonian H_{eff} in the k -space, where $v = 0.1$ and $\lambda = 0.392$. Here, $t_1 = 1$, $t_2 = 2$, and $N = 50$.

be written as

$$h_{\text{eff}}(k) = \begin{pmatrix} h_{11} & h_{12} \\ h_{21} & h_{22} \end{pmatrix} \quad (18)$$

with

$$\begin{aligned} h_{11} &= h_{\text{SSH}}(k) - ivI, \\ h_{12} &= i \frac{\lambda}{\sqrt{N_1}} \begin{pmatrix} 0 & t_1 + t_2 e^{-i(k+\pi)} \\ -[t_1 + t_2 e^{i(k+\pi)}] & 0 \end{pmatrix}, \\ h_{21} &= h_{12}, \\ h_{22} &= h_{\text{SSH}}(k) + ivI. \end{aligned} \quad (19)$$

Here, $k = 2\pi j/N_1$, $j = 1, 2, \dots, N_1$, $N_1 = N/2$, and $I = \begin{pmatrix} 1 & 0 \\ 0 & 1 \end{pmatrix}$. We present the complex energy spectrum from analytical solutions of the effective Hamiltonian H_{eff} and numerical solutions of the Hamiltonian $H = H_{\text{SSH}} + V$ in Fig. 11. We can see that they fit well, which manifests that the effective Hamiltonian we give in the Theorem 1 is feasible.

Secondly, the effective Hamiltonian of boundary states is expressed by $H_{\text{eff}} = I \otimes h_{\text{eff}}$, where

$$h_{\text{eff}} = iv\sigma_z + \sqrt{3}\sigma_y. \quad (20)$$

The eigenvalue is

$$E_{\text{eff}} = \pm \sqrt{3 - v^2}. \quad (21)$$

Likewise, we show numerical solutions of $H = H_{\text{SSH}} + V$ and analytical solutions of H_{eff} for boundary states in Fig. 12. We can see that H_{eff} agrees with $H = H_{\text{SSH}} + V$, which again confirms the rationality of Theorem 1. There is a \mathcal{PT} transition: in the case of $v < \sqrt{3}$, the eigenvalues are all real and at \mathcal{PT} -symmetry; and in the case of $v > \sqrt{3}$, the eigenvalues are all imaginary and at \mathcal{PT} -broken. At $v = \sqrt{3}$, boundary states are at the exceptional point with energy degeneracy, i.e., $E_{\text{eff}}(k) = 0$.

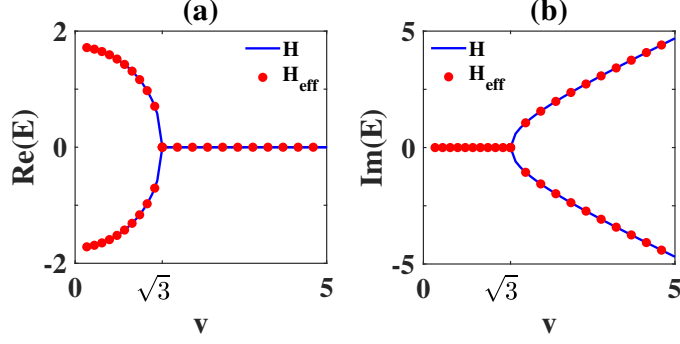


Fig. 12 The numerical solutions of boundary states from the Hamiltonian H in the real space and the analytical solutions of the effective Hamiltonian H_{eff} in the k -space, respectively. Here, $t_1 = 1$, $t_2 = 2$, and $N = 50$.

5 The Qi-Wu-Zhang model with the imaginary potential

In this section, we study the QWZ model with the imaginary potential to analyze the properties of two-dimensional topological systems with the imaginary potential.

The Hamiltonian of the QWZ model in the real space is

$$\begin{aligned}
H_{\text{QWZ}} = & \sum_{m_x=1}^{N_x-1} \sum_{m_y=1}^{N_y} (|m_x + 1, m_y\rangle \langle m_x, m_y| \otimes t_x + h.c.) \\
& + \sum_{m_x=1}^{N_x} \sum_{m_y=1}^{N_y-1} (|m_x, m_y + 1\rangle \langle m_x, m_y| \otimes t_y + h.c.) \\
& + u \sum_{m_x=1}^{N_x} \sum_{m_y=1}^{N_y} |m_x, m_y\rangle \langle m_x, m_y| \otimes \sigma_z,
\end{aligned} \tag{22}$$

where u is the staggered on site potential. The model describes a particle with two internal states hopping on a lattice where the nearest neighbour hopping is accompanied by an operation on the internal degree of freedom, and this operation is different for the hopping along the x-direction with $t_x = \frac{\sigma_z + i\sigma_x}{2}$ and y-direction with $t_y = \frac{\sigma_z + i\sigma_y}{2}$. The Hamiltonian in the k -space is

$$h_{\text{QWZ}}(k) = \sin k_x \cdot \sigma_x + \sin k_y \cdot \sigma_y + (\cos k_x + \cos k_y + u) \cdot \sigma_z, \tag{23}$$

and its eigenvalue is

$$E_{\pm}(k) = \pm \sqrt{(\sin k_x)^2 + (\sin k_y)^2 + (\cos k_x + \cos k_y + u)^2}. \tag{24}$$

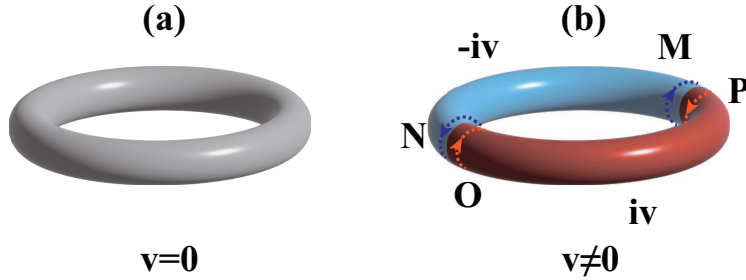


Fig. 13 The diagram of the Qi-Wu-Zhang model under the periodic conditions along the x-direction and y-direction. (a) represents the case without the imaginary potential. (b) represents the case with the imaginary potential. M, N, O, and P denote two sides of two interfaces, respectively. The arrow represents the direction of the wave vector of boundary states.

We consider the imaginary potential

$$\begin{aligned}
 V = & -iv \sum_{m_x=1}^{L/2} \sum_{m_y=1}^{N/2} |m_x, m_y\rangle \langle m_x, m_y| \otimes I \\
 & + iv \sum_{m_x=L/2+1}^L \sum_{m_y=N/2+1}^N |m_x, m_y\rangle \langle m_x, m_y| \otimes I
 \end{aligned} \tag{25}$$

for the QWZ model. The potential $-iv$ is applied to the left $N/2 \times L/2$ sites and the potential iv is applied to the right $N/2 \times L/2$ sites.

We consider the periodic boundary condition both along the x-direction and the y-direction, as plotted in Fig. 13. The complex energy spectra and eigenstates of the model are shown in Figs. 14 and 15. With an augment of the imaginary potential strength v , bulk states show separation within the \mathcal{PT} transition. After the separation of bulk states, the system appears some boundary states as reflected in Fig. 15. Each energy eigenvalue of the boundary state has two eigenstates, so here we only take one of the eigenstates in Fig. 15.

As the imaginary potential strength v continues to increase, these boundary states show non-Hermitian tearing with a \mathcal{PT} transition. As a result, the wave functions of boundary states, corresponding to the down energy band (represented by blue asterisks), are only localized at the side M or N of the interface in Fig. 15(c3). The wave functions of boundary states, corresponding to the up energy band (represented by red plus signs), are only localized at the position O or P of the interface in Fig. 15(c1). The direction of the wave vector of boundary states is parallel to the interfaces' direction, so boundary states appear decoupling. Additionally, we calculate the tearability and its derivative of the $j = 350$ and the $j = 450$ eigenstates in Fig. 16. There is a second-order phase transition about the tearability at the exceptional point.

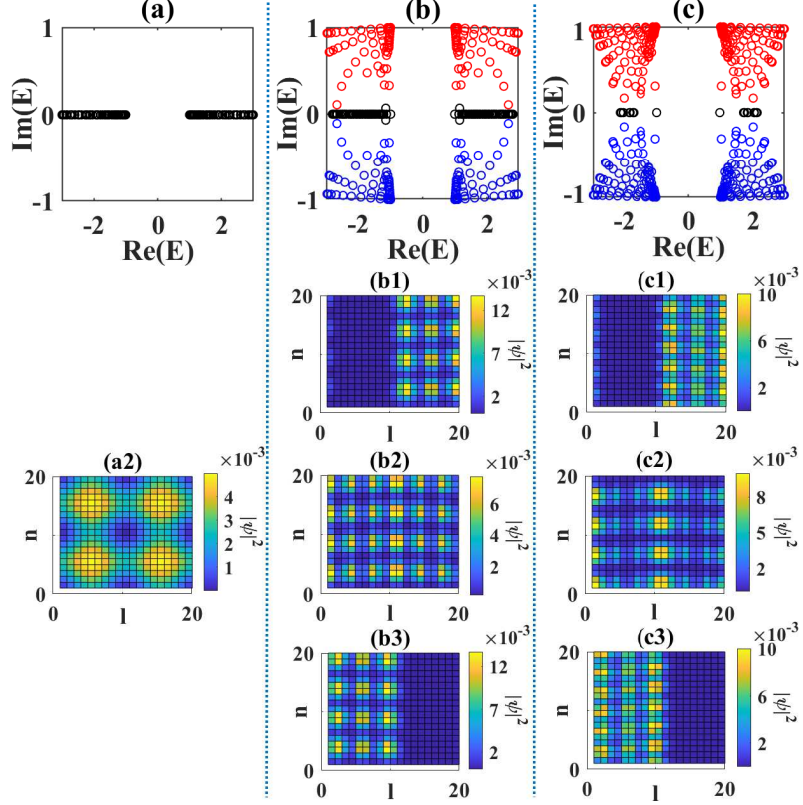


Fig. 14 (a), (b) and (c) are the complex energy spectra for different imaginary potential strengths $v = 0, 0.1$ and 0.21 , respectively. (a2) is a representative bulk state versus the site n and l for $v = 0$. (b1) to (b3) is a representative bulk state versus the site n and l corresponding to the energy eigenvalues represented by the red, black, and blue circles for $v = 0.1$, respectively. (c1) to (c3) is a representative bulk state versus the site n and l corresponding to the energy eigenvalues represented by the red, black, and blue circles for $v = 0.21$, respectively. Here, $N = L = 20$ and $u = -1$.

Following Theorem 1, we provide the effective Hamiltonian for this situation. The effective Hamiltonian of bulk states can be described by

$$h_{\text{eff}} = \begin{pmatrix} h_{11} & h_{12} \\ h_{21} & h_{22} \end{pmatrix}, \quad (26)$$

where

$$h_{11} = h_{\text{QWZ}}(k) - ivI, \quad (27)$$

$$h_{12} = \frac{\lambda_1}{\sqrt{L_1}} \left[\sin(k_x + \pi) \cdot \sigma_x + \cos\left(k_x + \frac{\pi}{2}\right) \cdot \sigma_z \right],$$

$$h_{21} = h_{12}, \quad (27)$$

$$h_{22} = h_{\text{QWZ}}(k) + ivI. \quad (28)$$

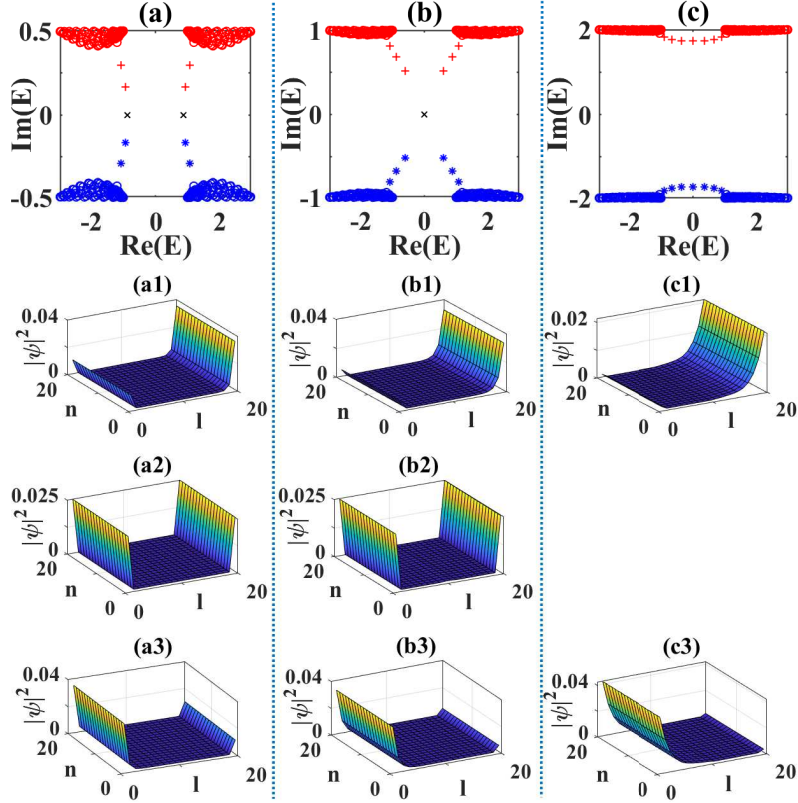


Fig. 15 (a), (b) and (c) are the complex energy spectra for different imaginary potential strengths $v = 0.5, 1$ and 2 , respectively. (a1) to (a3) is a representative boundary state versus the site n and l corresponding to the energy eigenvalues represented by the red plus signs, black crosses, and blue asterisks for $v = 0.5$, respectively. (b1) to (b3) is a representative boundary state versus the site n and l corresponding to the energy eigenvalues represented by the red plus signs, black crosses, and blue asterisks for $v = 1$, respectively. (c1) and (c3) are the representative boundary states versus the site n and l corresponding to the energy eigenvalues represented by the red plus signs and blue asterisks for $v = 2$, respectively. Here, $N = L = 20$ and $u = -1$.

λ_1 is the fitting parameter. Here, $k_x = 2\pi j_x/L_1$, $j_x = 1, 2, \dots, L_1$, and $L_1 = L/2$. $k_y = 2\pi j_y/N$, $j_y = 1, 2, \dots, N$. For the boundary states, the effective Hamiltonian is

$$h_{\text{eff}} = \begin{pmatrix} -\sin k_y - iv & \lambda_2 \\ \lambda_2 & \sin k_y + iv \end{pmatrix}, \quad (29)$$

where λ_2 is a fitting parameter. The numerical solutions of the Hamiltonian $H = H_{\text{QWZ}} + V$ in the real space and analytical solutions of the effective Hamiltonian H_{eff} in the k -space for bulk states and boundary states are shown in Fig. 17. Roughly, the solutions of effective Hamiltonian are in agreement with numerical results.

For an arbitrary dimensional model $h_0(k_\perp, \vec{k}_{//})$ with the imaginary potential, in which the potential $-iv$ is applied to the left $L/2$ sites and the potential iv is applied

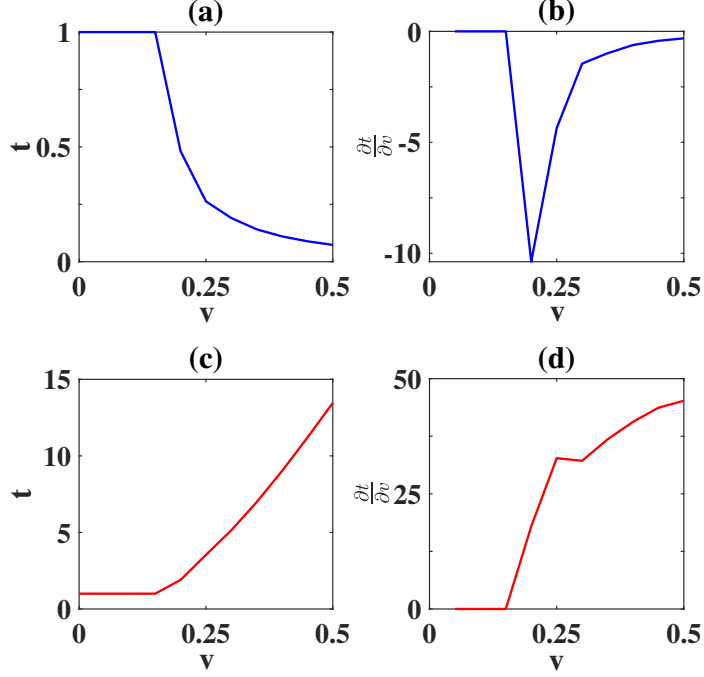


Fig. 16 The tearability t and the derivative $\frac{\partial t}{\partial v}$ of the Qi-Wu-Zhang model. (a) and (b) are t and $\frac{\partial t}{\partial v}$ of the $j = 350$ eigenstate, respectively. (c) and (d) are t and $\frac{\partial t}{\partial v}$ of the $j = 450$ eigenstate, respectively. Here, $N = L = 20$ and $u = -1$.

to the right $L/2$ sites, the effective Hamiltonian of bulk states is

$$h_{\text{eff}}(k_{\perp}, \vec{k}_{//}) = \begin{pmatrix} h_0(k_{\perp}, \vec{k}_{//}) - ivI & \frac{\alpha(k_{\perp}, \vec{k}_{//})}{\sqrt{L/2}} \\ \frac{\alpha(k_{\perp}, \vec{k}_{//})}{\sqrt{L/2}} & h_0(k_{\perp}, \vec{k}_{//}) + ivI \end{pmatrix}, \quad (30)$$

where $k_{\perp} = 2\pi j/L_1$, $j = 1, 2, \dots, L_1$, and $L_1 = L/2$. I is a unit operator. If this model is also topological, then it would disappear boundary states after the bulk states show separation. The effective Hamiltonian of these boundary states is

$$h_{\text{eff}}(\vec{k}_{//}) = \begin{pmatrix} h_0(\vec{k}_{//}) - ivI & \lambda I \\ \lambda I & -h_0(\vec{k}_{//}) + ivI \end{pmatrix}, \quad (31)$$

where λ is a fitting parameter related to v .

6 Conclusions

In the paper, we study the non-Hermitian system under dissipation, where the left and right sites are subject to different imaginary potentials. To better understand

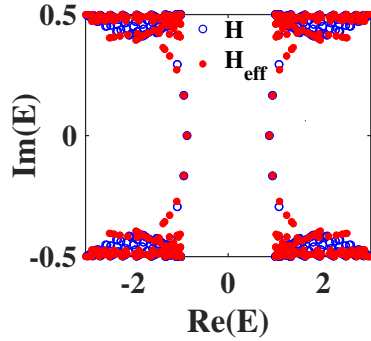


Fig. 17 The complex energy spectra from numerical solutions of the Hamiltonian H in the real space and solutions of the effective Hamiltonian H_{eff} in the k -space, where $v = 0.5$, $\lambda_1 = 0.75$ and $\lambda_2 = 0.9999$.

the physical phenomena of the total system, we give a series of the effective 2×2 Hamiltonian in the k -space by reducing the $N \times N$ Hamiltonian in the real space. We discover that the energy band shows an imaginary line gap with the imaginary potential. Based on this phenomenon, the theory of non-Hermitian tearing is proposed, in which the system is either in the partial tearing or complete tearing accompanied by a \mathcal{PT} transition. To describe the effect of different imaginary potentials on an eigenstate, we define tearability. According to the relationship between the interface's direction and the direction of the wave vector of eigenstates, separation and decoupling are introduced. By the theory of non-Hermitian tearing, we explore the physical properties of the simple one-dimensional tight binding model, one-dimensional SSH model and QWZ model. The results show that in the process of non-Hermitian tearing, the system has the following properties:

1. bulk states show separation;
2. after the separation of bulk states, topological systems could appear boundary states and these boundary states show decoupling;
3. the tearability exhibits a continuous phase transition at the exceptional point;
4. if the model adds the nonreciprocal hopping, then bulk states will display skin effect in the bound region, which will be our next study.

In the future, we will further study the non-Hermitian tearing in more complex systems and the relationship with other non-Hermitian phenomena.

Acknowledgements. This work was supported by NSFC (Grant No. 11974053, 12174030) and the National Key R&D Program of China (Grant No.2023YFA1406704).

Author contribution statement. Qian Du and Su-Peng Kou contributed to the analysis and writing of the manuscript. Qian Du and Xin-Ran Ma contributed to the calculation of the manuscript. Every author has discussed and reviewed the manuscript before submission.

Data Availability Statement This manuscript has no associated date or the date will not be deposited.

Appendix A The probability and tearability of eigenstates of the effective Hamiltonian

For the simple one-dimensional tight binding model with the imaginary potential, $h_{\text{eff}}(k)$ is expressed as

$$h_{\text{eff}}(k) = \begin{pmatrix} E_0 - iv & \alpha \\ \alpha & E_0 + iv \end{pmatrix}, \quad (\text{A1})$$

where $\alpha = \frac{2t \sin k}{\sqrt{N_1}} \cdot \lambda$ and λ is a fitting parameter related to v . The eigenvalues are

$$E_{\text{eff}} = E_0 \pm \sqrt{\alpha^2 - v^2}. \quad (\text{A2})$$

The eigenstates are

$$\Psi_+ = \frac{1}{A} \begin{pmatrix} 1 \\ \frac{iv + \sqrt{\alpha^2 - v^2}}{\alpha} \end{pmatrix}, \Psi_- = \frac{1}{B} \begin{pmatrix} 1 \\ \frac{iv - \sqrt{\alpha^2 - v^2}}{\alpha} \end{pmatrix}, \quad (\text{A3})$$

where $A = \sqrt{1 + \left(\frac{iv + \sqrt{\alpha^2 - v^2}}{\alpha}\right)^2}$ and $B = \sqrt{1 + \left(\frac{iv - \sqrt{\alpha^2 - v^2}}{\alpha}\right)^2}$. The corresponding probabilities are

$$\begin{aligned} \rho_{+,L} &= \frac{\alpha^2}{\alpha^2 + (iv + \sqrt{\alpha^2 - v^2})^2}, \\ \rho_{+,R} &= \frac{(iv + \sqrt{\alpha^2 - v^2})^2}{\alpha^2 + (iv + \sqrt{\alpha^2 - v^2})^2}, \\ \rho_{-,L} &= \frac{\alpha^2}{\alpha^2 + (iv - \sqrt{\alpha^2 - v^2})^2}, \\ \rho_{-,R} &= \frac{(iv - \sqrt{\alpha^2 - v^2})^2}{\alpha^2 + (iv - \sqrt{\alpha^2 - v^2})^2}. \end{aligned} \quad (\text{A4})$$

The tearability are

$$\begin{aligned} t_+ &= \frac{(iv + \sqrt{\alpha^2 - v^2})^2}{\alpha^2}, \\ t_- &= \frac{(iv - \sqrt{\alpha^2 - v^2})^2}{\alpha^2}. \end{aligned} \quad (\text{A5})$$

References

1. C. E. Rüter, K. G. Makris, R. El-Ganainy, D. N. Christodoulides, M. Segev, and D. Kip, Observation of parity–time symmetry in optics, *Nat. Phys.* **6**, 192 (2010)
2. A. Guo, G. J. Salamo, D. Duchesne, R. Morandotti, M. Volatier-Ravat, V. Aimez, G. A. Siviloglou, and D. N. Christodoulides, Observation of \mathcal{PT} -Symmetry Breaking in Complex Optical Potentials *Phys. Rev. Lett.* **103**, 093902 (2009)
3. Y. D. Chong, L. Ge, and A. D. Stone, \mathcal{PT} -Symmetry Breaking and Laser-Absorber Modes in Optical Scattering Systems, *Phys. Rev. Lett.* **106**, 093902 (2011)
4. R. El-Ganainy, K. G. Makris, M. Khajavikhan, Z. H. Musslimani, S. Rotter, and D. N. Christodoulides, Non-Hermitian physics and PT symmetry, *Nat. Phys.* **14**, 11 (2018)
5. L. Feng, Y.-L. Xu, W. S. Fegadolli, M.-H. Lu, J. E. B. Oliveira, V. R. Almeida, Y.-F. Chen, and A. Scherer, Experimental demonstration of a unidirectional reflectionless parity-time metamaterial at optical frequencies, *Nat. Mater.* **12**, 108 (2013)
6. H. Hodaei, M.-A. Miri, M. Heinrich, D. N. Christodoulides, and M. Khajavikhan, Parity-time-symmetric microring lasers, *Science* **346**, 975 (2014)
7. L. Feng, Z. J. Wong, R.-M. Ma, Y. Wang, and X. Zhang, Single mode laser by parity-time symmetry breaking, *Science* **346**, 972 (2014)
8. W. Song, W. Sun, C. Chen, Q. Song, S. Xiao, S. Zhu, and T. Li, Breakup and Recovery of Topological Zero Modes in Finite Non-Hermitian Optical Lattices, *Phys. Rev. Lett.* **123**, 165701 (2019)
9. V. Kozii and L. Fu, Non-Hermitian Topological Theory of Finite-Lifetime Quasiparticles: Prediction of Bulk Fermi Arc due to Exceptional Point, [arXiv:1708.05841](https://arxiv.org/abs/1708.05841)
10. Z. Gong, Y. Ashida, K. Kawabata, K. Takasan, S. Higashikawa, and M. Ueda, Topological Phases of Non Hermitian Systems, *Phys. Rev. X* **8**, 031079 (2018)
11. H. Shen, B. Zhen, and L. Fu, Topological Band Theory for Non-Hermitian Hamiltonians, *Phys. Rev. Lett.* **120**, 146402 (2018)
12. F. Song, S. Yao, and Z. Wang, Non-Hermitian Topological Invariants in Real Space, *Phys. Rev. Lett.* **123**, 246801 (2019)
13. N. Matsumoto, K. Kawabata, Y. Ashida, S. Furukawa, and M. Ueda, Continuous Phase Transition without Gap Closing in Non-Hermitian Quantum Many-Body Systems, *Phys. Rev. Lett.* **125**, 260601 (2020)

14. K. Kawabata, K. Shiozaki, M. Ueda, and M. Sato, Symmetry and Topology in Non-Hermitian Physics, *Phys. Rev. X* **9**, 041015 (2019)
15. K. Kawabata, K. Shiozaki, and S. Ryu, Topological Field Theory of Non-Hermitian Systems, *Phys. Rev. Lett.* **126**, 216405 (2021)
16. Y. Michishita and R. Peters, Equivalence of Effective Non-Hermitian Hamiltonians in the Context of Open Quantum Systems and Strongly Correlated Electron Systems, *Phys. Rev. Lett.* **124**, 196401 (2020)
17. C. M. Bender, D. C. Brody, and H. F. Jones, Complex Extension of Quantum Mechanics, *Phys. Rev. Lett.* **89**, 270401 (2002)
18. I. Rotter, A non-Hermitian Hamilton operator and the physics of open quantum systems, *J. Phys. A: Math. Theor.* **42**, 153001 (2009)
19. F. Reiter and A. S. Sørensen, Effective operator formalism for open quantum systems, *Phys. Rev. A* **85**, 032111 (2012)
20. A. Mostafazadeh, Pseudo-Hermiticity versus PT symmetry: The necessary condition for the reality of the spectrum of a non-Hermitian Hamiltonian *J. Math. Phys.* **43** 205 (2002); A. Mostafazadeh, Pseudo-Hermiticity versus PT-symmetry. II. A complete characterization of non-Hermitian Hamiltonians with a real spectrum, *ibid*, **43** 2814 (2002); A. Mostafazadeh A, Pseudo-Hermiticity versus PT-symmetry III: Equivalence of pseudo-Hermiticity and the presence of antilinear symmetries, *ibid*, **43** 3944, (2002)
21. N. Moiseyev, *Non-Hermitian Quantum Mechanics* (Cambridge University Press, Cambridge, 2011)
22. Y. Ashida, Z. Gong, and M. Ueda, Non-Hermitian physics, *Adv. Phys.* **69**, 249 (2020)
23. C. M. Bender, Making sense of non-Hermitian Hamiltonians, *Rep. Prog. Phys.* **70**, 947 (2007).
24. G. Gamow, Zur Quantentheorie des Atomkernes, *Z. Phys.* **51**, 204 (1928)
25. P. M. Radmore and P. L. Knight, Population trapping and dispersion in a three-level system, *J. Phys. B: Atom. Mol. Phys.*, **15**, 561 (1982)
26. R. M. More, Theory of decaying states, *Phys. Rev. A* **4**, 1782 (1971)
27. N. Hatano and D. R. Nelson, Localization Transitions in Non-Hermitian Quantum Mechanics, *Phys. Rev. Lett.* **77**, 570 (1996)
28. C. M. Bender, and S. Boettcher, *Phys. Rev. Lett.* **80**, 5243 (1998)

29. V. M. Martinez Alvarez, J. E. Barrios Vargas, and L. E. F. Foa Torres, Non-Hermitian robust edge states in one dimension: Anomalous localization and eigenspace condensation at exceptional points, *Phys. Rev. B* **97**, 121401(R) (2018)
30. S. Yao and Z. Wang, Edge States and Topological Invariants of Non-Hermitian Systems, *Phys. Rev. Lett.* **121**, 086803 (2018)
31. L. Li, C. H. Lee, S. Mu, and J. Gong, Critical non-Hermitian skin effect, *Nat. Commun.* **11**, 5491 (2020)
32. K. Kawabata, M. Sato, and K. Shiozaki, Higher-order non-hermitian skin effect, *Phys. Rev. B* **102**, 205118 (2020)
33. D. S. Borgnia, A. J. Kruchkov, and R.-J. Slager, Non-Hermitian Boundary Modes and Topology, *Phys. Rev. Lett.* **124**, 056802 (2020)
34. N. Okuma, K. Kawabata, K. Shiozaki, and M. Sato, Topological Origin of Non-Hermitian Skin Effects, *Phys. Rev. Lett.* **124**, 086801 (2020)
35. Y. Xiong, Why does bulk boundary correspondence fail in some non-hermitian topological models, *J. Phys. Commun.* **2** 035043 (2018)
36. T. E. Lee, Anomalous Edge State in a Non-Hermitian Lattice, *Phys. Rev. Lett.* **116**, 133903 (2016)
37. F. K. Kunst, E. Edvardsson, J. C. Budich, and Emil J. Bergholtz, Biorthogonal Bulk-Boundary Correspondence in Non-Hermitian Systems, *Phys. Rev. Lett.* **121**, 026808 (2018)
38. S. Yao, F. Song and Z. Wang, Non-Hermitian Chern Bands, *Phys. Rev. Lett.* **121**, 136802 (2018)
39. H.-G. Zirnstein, G. Refael, and B. Rosenow, Bulk Boundary Correspondence for Non-Hermitian Hamiltonians via Green Functions, *Phys. Rev. Lett.* **126**, 216407 (2021)
40. X.-R. Wang, C.-X. Guo, and S.-P. Kou, Defective edge states and number-anomalous bulk-boundary correspondence in non-Hermitian topological systems, *Phys. Rev. B* **101**, 121116(R) (2020)
41. H. Zhao, X. Qiao, T. Wu, B. Midya, S. Longhi, and L. Feng, Non-Hermitian topological light steering, *Science* **365**, 1163 (2019)
42. Y. Li, C. Fan, X.g Hu, Y. Ao, C. Lu, C. T. Chan, D. M. Kennes, and Q. Gong, Effective Hamiltonian for Photonic Topological Insulator with Non-Hermitian Domain Walls, *Phys. Rev. Lett.* **129**, 053903 (2022)

43. Y.-J. Wu, C.-C. Liu and J. Hou, Wannier-type photonic higher-order topological corner states induced solely by gain and loss, *Phys. Rev. A* **101**, 043833 (2020)
44. D. Halder, S. Ganguly, and S. Basu, Properties of the non-Hermitian SSH model: role of \mathcal{PT} symmetry, *J. Phys.: Condens. Matter* **35**, 105901 (2023)
45. S. Jana, and L. Sirota, Emerging exceptional point with breakdown of skin effect in non-Hermitian systems, arXiv:2303.15050v2 (2023)
46. T.-S. Deng and W. Yi, Non-Bloch topological invariants in a non-Hermitian domain wall system, *Phys. Rev. B* **100**, 035102 (2019)
47. J.-R. Li, C. Luo, L.-L. Zhang, S.-F. Zhang, P.-P. Zhu, and W.-J. Gong, Band structures and skin effects of coupled nonreciprocal Su-Schrieffer-Heeger lattices, *Phys. Rev. A* **107**, 022222 (2023)
48. C.-X. Guo, X. Wang, H. Hu, and S. Chen, Accumulation of scale-free localized states induced by local non-Hermiticity, *Phys. Rev. B* **107**, 134121 (2023)
49. B. Li, H.-R. Wang, F. Song and Z. Wang, Scale-free localization and \mathcal{PT} symmetry breaking from local non-hermiticity, arXiv:2302.04256v1 (2022)
50. X.-R. Ma, K. Cao, X.-R. Wang, Z. Wei, Q. Du, S.-P. Kou, Non-Hermitian Chiral Skin Effect, *Phys. Rev. Res.* **6**, 013213(2024)